Dynamical stability of the alpha and theta phases of alumina

Lodziana, Zbigniew; Parlinski, K.

Published in:
Physical Review B Condensed Matter

Link to article, DOI:
10.1103/PhysRevB.67.174106

Publication date:
2003

Document Version
Publisher's PDF, also known as Version of record

Dynamical stability of the α and θ phases of alumina

Z. Łodziana
Center for Atomic-scale Materials Physics, DTU, Building 307, DK-2800 Lyngby, Denmark

K. Parliński
Institute of Nuclear Physics, ul. Radzikowskiego 152, 30-142 Kraków, Poland

(Received 7 November 2002; published 16 May 2003)

Using density functional calculations the phonon dispersion relations, phonon density of states, and free energy of θ and α phases of alumina are investigated. The temperature dependence of the free energy indicates that entropy contributes to the destabilization of the α phase at the high temperatures, but this is insufficient to drive transformations between those two phases. The fcc arrangement of the oxygen sublattice plays an important role in the stabilization of the θ phase above 600 K. The present calculations explain the common presence of tetrahedrally coordinated Al cations in alumina, and suggest that some other than entropic mechanism exists, which stabilizes transition aluminas up to 1400 K. The present calculations go beyond the ground state energy calculations [C. Wolverton and K.C. Hass, Phys. Rev. B **63**, 24102 (2001)], and give an additional understanding of the stability of transition alumina at finite temperatures.

DOI: 10.1103/PhysRevB.67.174106 PACS number(s): 61.43.Bn

I. INTRODUCTION

Alumina is an extremely important material due to its great hardness, high thermal stability, and chemical inertness. These properties lead to applications in the catalytic and coating industries.[1] Aluminum oxide (Al_2O_3) exists in various structural polymorphs, which are stable over a wide range of temperatures. Besides the most stable α-alumina (corundum, sapphire) there exists a variety of so-called transition phases.[1,2] These phases (denoted as $\gamma,\eta,\delta,\theta$) usually are formed prior to corundum, when an oxide is obtained via the dehydration process, and they are very stable up to 1100 °C. The sequence $\gamma\rightarrow\delta\rightarrow\theta\rightarrow\alpha$[3] occurs as the temperature increases, when the alumina is obtained from either hydroxide (boehmite) or melt. All transition phases possess very low degree of crystallinity with surface area higher than 150 m^2/g, preserved up to the stability limit. The α-phase, on the other hand, usually forms single crystals.[2]

During the past years an enormous scientific effort has been focused on the understanding of the nature, properties, and transition sequence of alumina. Despite this, many questions are still left unanswered. Especially puzzling is the stability of the transition phases.

Although the details of the atomic structure of transition aluminas are still under discussion,[1,4–6] there seem to be an agreement that the γ, δ, and η phases possess a defected spinel structure. The oxygen atoms in the transition phases are arranged into a slightly distorted fcc sublattice, while the cations are distributed between octahedral and tetrahedral sites. The distribution of cations and vacancies within a spinel structure is still being debated in the literature, but the preferential occupancy of O_h sites by the vacancies seems to be favored. For a detailed discussion of problems related to the transition aluminas the reader may refer to the excellent review by Wolverton and Hass.[5] The θ phase is the ultimate ground state of transition structures, which always appear just prior to the transformation to the corundum. The main structural differences between corundum and the transition phases are a hcp structure of the oxygen sublattice and the only octahedral coordination of the aluminum in the α phase.

In the present study, we provide insight into the question of how the free energy contributes to the stability of corundum with respect transition phases, which we represent here by θ-alumina. We also consider the role of the vibrational entropy in the stabilization of the transition alumina at high temperatures. The analysis of the transition alumina ground state properties[5] ruled out the hydrogenated spinel as a candidate for the spinel based alumina, and showed the tendency of Al to occupy tetrahedral sites. In the present studies we go beyond the ground state, providing some insight into the stability of transition aluminas at finite temperatures. By means of extensive density functional theory (DFT) calculations, we show that at low temperatures the vibrational free energy of corundum is lower than that of θ-alumina, while above $T>600$ K, this situation reverses. The origin of this phenomena is traced to the result of the presence of a fcc arrangement of the oxygen sublattice, which possesses a larger vibrational entropy at high temperatures.

The structure of the α-Al_2O_3 belongs to the rhombohedral space group $R\bar{3}c$. The unit cell contains two formula units; see Fig. 1(a). The representation of the structure in a hexagonal unit cell (six formula units) visualizes the layered structure of corundum. Oxygen is arranged in layers perpendicular to the c axis, and aluminum occupy octahedral interstices between oxygen sheets. The stoichiometry requires that 1/3 of the octahedral sites are vacant. The θ-Al_2O_3 possesses a monoclinic structure belonging to the $C2/m$ space group (a structure that is pseudomorphic with β-Ga_2O_3). The unit cell contains four formula units [cf. Fig. 1(b)]. In this phase, oxygen forms a slightly distorted fcc lattice and cations evenly occupy tetrahedral and octahedral interstices.

Below in Sec. II the methods of calculations are presented, followed by a presentation of the results related to the static structures and the vibrational spectrum of aluminas. Then the thermodynamics of both phases is discussed in some more detail. The paper is completed with a discussion.

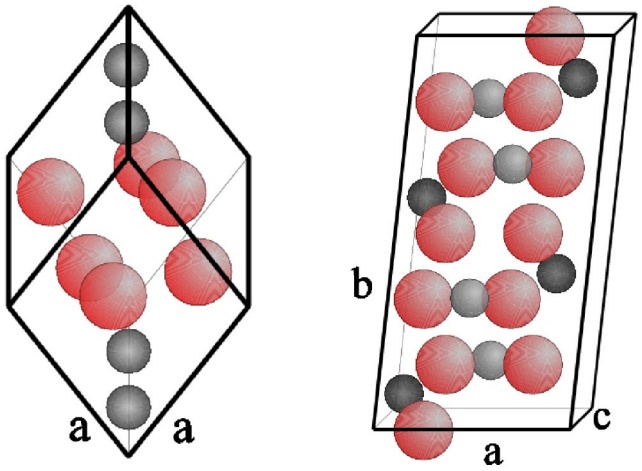

FIG. 1. (Color online) Schematic representation of the rhombohedral unit cell of α-Al_2O_3 (left), and θ alumina (right). Large red spheres represent oxygen, small gray are for aluminum. On (b) darker gray spheres denote tetrahedrally coordinated Al.

II. METHOD

The structure and dynamics of the θ- and α-Al_2O_3 were calculated within the DFT approach.[7] The ionic cores are represented by ultrasoft pseudopotentials. The electronic density is determined by an iterative diagonalization of the Kohn-Sham Hamiltonian, and the resulting Kohn-Sham eigenstates are populated according to the Fermi statistics with a finite temperature smearing of $T=0.02$ eV. The Pulay mixing of the resulting densities is applied and the procedure is repeated until a self-consistency of the electronic density is achieved. Then the total energy is extrapolated to $T=0$ K. The calculations were carried within a generalized gradient (GGA) PW91 (Ref. 8) approximation of the exchange correlation function. A very restrictive accuracy was applied to compare the relative stability of both phases at $T=0$ K. The wave function was sampled according to a Monkhorst-Pack scheme with a *k*-point meshes of $4\times4\times4$ for the α phase and $2\times8\times4$ for the θ phase. This is sufficient to compare ground state energies of both phases, as the denser grid, $8\times8\times8$ for the α phase and $4\times10\times6$ for the θ phase changes the ground state energy by less than 0.0007 eV/formula unit. For the calculations of the lattice dynamics, a larger supercell had to be used to assure that the force constants fall sufficiently with distance. For the α phase, the supercell of $2\times2\times2$ was found to be sufficient, and for the θ-Al_2O_3 the $1\times3\times2$ supercell gives a satisfactory decay of the interatomic force constants. Thus calculations were performed on systems of 80 and 120 atoms for α and θ phases, respectively. For the calculations on those large systems the *k*-point sampling was limited to the Γ point, which only slightly affects the accuracy of the small supercell. The cutoff of the kinetic energy in all cases was 490 eV. The structure was optimized according to the calculated Hellmann-Feynman forces. Both internal positions of atoms and the unit cell parameters were optimized.

The lattice dispersion relations are determined by the direct method.[9] The details of this method are presented elsewhere,[10] but here we briefly mention that the method utilizes Hellmann-Feynmann forces acting on atoms in the supercell. To determine the dynamical matrix, three independent displacements of the amplitude ±0.03 Å along *x*, *y*, and *z* directions for every symmetry nonequivalent atom were calculated. All displaced configurations generate 1440 (α) and 2160 (θ) components of the Hellmann-Feynman forces. Next, the symmetry of the force constants, following from $R\bar{3}c$ and $C2/m$ space groups of α and θ phases' is established. The force constants are fitted to the collected Hellmann-Feynman forces by the singular value decomposition method. At the distance of 7 Å, the largest element of the force constant is three orders of magnitude smaller than the corresponding one from the first shell. The diagonalization of the dynamical matrix provides the phonon frequencies.

The method is correct for the analytical part of the dynamical matrix only, as the periodic boundary conditions are imposed on the supercell. The large band gap (8 eV) causes incomplete screening in alumina, reflected by Born effective charges carried by ions. Thus, the nonanalytical part describes the effects of this macroscopic electrostatic field that arises for certain infrared (IR) modes in the long wavelength limit ($\mathbf{q}\rightarrow0$). The symbol $\mathbf{q}$ is used to distinguish vibrational modes from the electronic states sampling in reciprocal space. A Coulomb interaction splits this mode into longitudinal (LO) and transversal optical (TO) parts, lifting the LO-TO degeneracy. We account for the nonanalytical part of dynamical matrix by introducing the effective charges following Ref. 11. The values of the screened Born effective charge tensors ($Z_{\alpha\beta}/\sqrt{\epsilon_{zz}^{\infty}}$) are $Z_{xx}=Z_{yy}=1.65$ and $Z_{zz}=1.63$ for Al, and $Z_{xx}=-1.15$, $Z_{yy}=-1.04$, and $Z_{zz}=-1.09$ for oxygen. The two independent elements of the dielectric tensor are $\epsilon_{xx}=\epsilon_{yy}=3.2$ and $\epsilon_{zz}=3.1$. This procedure affects only LO IR modes.

III. RESULTS

At a preliminary step the unit cells of both phases of Al_2O_3 were optimized. The optimization was carried in the symmetry appropriate for each phase; the internal atomic positions and the lattice parameters were relaxed. After a convergence with respect to the forces exerted on atoms was accomplished, the symmetry was released and structures were reoptimized. Both corundum and θ-alumina remain in the ground state of the first optimization stage. The largest residual force exerted on the atom was smaller than 0.0001 eV/Å at the end of this process. The lattice parameters and the energy difference between phases are presented in Table I. The calculated lattice constants are in the level of agreement with experimental data typical for GGA calculations. The internal positions of atoms agree precisely with the experimentally measured position for corundum. The agreement between previous and present calculations is very good. The ground state energies of both phases are very similar, slightly (by 0.03 eV/Al_2O_3) favoring corundum. The previous calculations[5] gave similar result, showing also that the local density approximation exchange-correlation functional tend to overestimate $\Delta E(\alpha-\theta)$ at $T=0$.[5] The insight into

TABLE I. Comparison of the calculated and literature structural parameters of the α and θ alumina. The ground state energy differences are given in (meV/formula unit), and are calculated from a converged $1\times1\times1$ supercell.

α-Al_2O_3	Present	Calc. (Ref. 5)	Expt. (Ref. 12)
a (Å)	5.153	5.161	5.128
α (deg)	55.279	55.27	55.28
Al (x,x,x)	0.352	0.352	0.352
O $(z,\overline{z}+\frac{1}{2},\frac{1}{2})$	0.556	0.556	0.556
θ-Al_2O_3	Present	Calc. (Ref. 5)	Expt. (Ref. 4)
a (Å)	11.853	11.86	11.85
b (Å)	2.923	2.929	2.904
c (Å)	5.631	5.657	5.622
β (deg)	104.034	104.0	103.8
O $(x,0,z)$	(0.161,0.108)	(0.159,0.109)	(0.161,0.098)
O $(x,0,z)$	(0.495,0.257)	(0.495,0.257)	(0.495,0.253)
O $(x,0,z)$	(0.826,0.433)	(0.826,0.432)	(0.827,0.427)
Al $(x,0,z)$	(0.909,0.205)	(0.910,0.204)	(0.917,0.207)
Al $(x,0,z)$	(0.658,0.316)	(0.658,0.317)	(0.660,0.316)
$\Delta E(\theta-\alpha)$ (meV)	30	40	<120

the energy difference between both phases of alumina is of particular interest and will be addressed below.

The enlarged supercells for the lattice dynamics calculations were constructed from the optimized structures described above and only the internal atomic coordinates were reoptimized. Since the multiplication of the unit cell folds back the residual forces, the reoptimization of the internal atomic coordinates lifts the problem of losing accuracy. The residual forces remained below 0.0001 eV/Å for both phases.

A. Phonon dispersion relations

The calculated phonon spectrum along some high symmetry directions is presented in Fig. 2(a) for α-alumina and in Fig. 2(b) for θ-alumina. The spectrum has a rather complicated structure, as there are 30 different branches. The important feature to note is that all frequencies presented in Fig. 2 are positive. This is not a surprise for corundum, however for the θ-Al_2O_3 this is an indication that the structure is dynamically stable in a crystalline phase. Another important property can be observed when comparing Figs. 2(a) and 2(b) at the range of 18 to 23 THz. A higher density of phonon branches exists for the θ alumina in this range.

The rich literature of the vibrational properties of corundum[11,13–16] gives an opportunity for a better comparison of our results and existing data. The phonon dispersion relations were determined experimentally by inelastic neutron scattering,[15] and are presented as squares in Fig. 2(a). The overall agreement is in the typical range of *ab initio* calculations.

The Γ point frequencies for corundum are summarized in Table II. In the long wavelength limit ($\mathbf{q}=0$), the vibrational frequencies are determined via infrared and Raman measure-

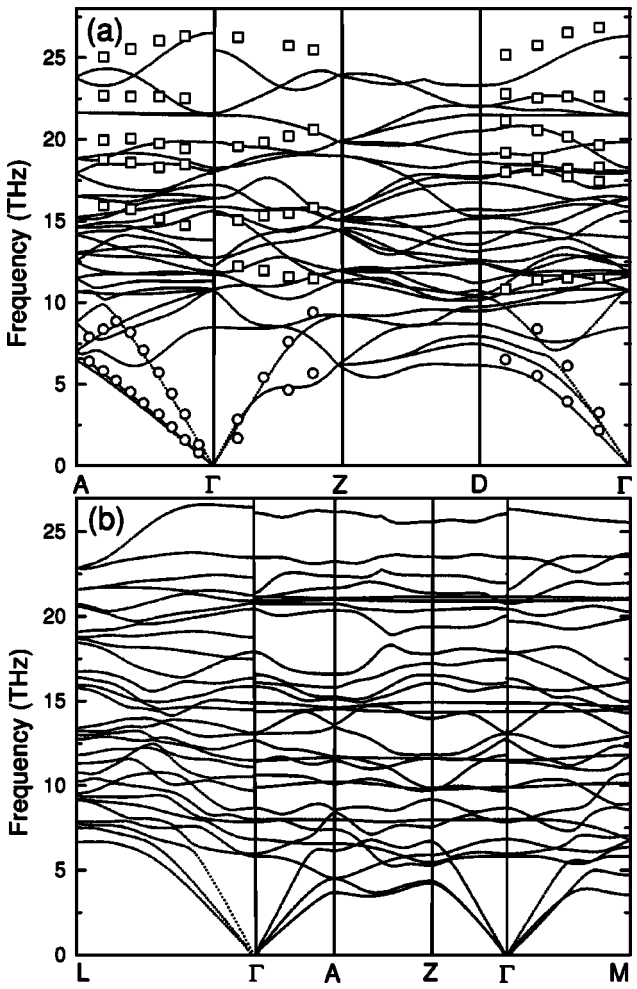

FIG. 2. Phonon dispersion relations for (a) α-alumina. High symmetry points are $Z=(\frac{1}{2},\frac{1}{2},\frac{1}{2})$, $A=(0,\frac{1}{2},0)$, and $D=(\frac{1}{2},0,\frac{1}{2})$. (b) θ-alumina with high symmetry points: $L=(\frac{1}{2},0,\frac{1}{2})$, $A=(0,0,\frac{1}{2})$, $Z=(\frac{1}{2},\frac{1}{2},0)$, and $M=(\frac{1}{2},\frac{1}{2},\frac{1}{2})$. Lines represent calculated spectrum and points represent experimental data (Ref. 15).

ments. The accuracy of these experiments is superior to the scattering measurements presented in Fig. 2(a). All modes are classified following the space group analysis and six IR and seven Raman modes are allowed by the symmetry. Our calculations for the Raman frequencies (Table II) agree with the experimental values within 5%, which is typical when using the direct method. For the IR frequencies, the correspondence of the calculated TO frequencies to the experiment is good, and the good agreement for LO modes assures that our choice of the treatment of the screening effects is correct. The systematic underestimation of the frequencies can be attributed to slight overestimation of the unit cell volume by GGA calculations.

The good agreement between the experimental and calculated vibrational spectra of corundum justifies our calculations and allows the extension to the θ phase, where experimental data are not available. The Γ-point frequencies for this phase are collected in Table III. Even though any experimental details of the microscopic dynamics are not known, there is an interesting property of transition alumina, which relates lattice dynamics of θ-Al_2O_3 to another known struc-

TABLE II. The comparison of the calculated and literature frequencies of the corundum optical modes at $\mathbf{q}=\Gamma$ point. For IR modes the longitudinal frequencies (LO) are given in parentheses. Frequencies are given in THz.

Mode	Present	Expt. (Ref. 13)	Calc. (Ref. 11)
A2u(I)	10.985 (15.37)	11.99 (15.35)	11.72 (14.98)
A2u(I)	15.846 (25.32)	17.48 (26.11)	17.14 (25.79)
Eu(I)	10.640 (11.49)	11.54 (11.63)	11.44 (11.50)
Eu(I)	12.179 (13.87)	13.25 (14.39)	13.05 (14.41)
Eu(I)	15.660 (17.71)	17.06 (18.74)	16.95 (18.74)
Eu(I)	17.778 (26.40)	19.04 (26.98)	18.83 (26.60)
	Present	Expt. (Ref. 14)	Calc. (Ref. 11)
Eg(R)	10.734	11.3	11.38
Eg(R)	11.974	13.0	12.86
Eg(R)	12.602	13.5	13.27
Eg(R)	16.089	17.3	17.02
Eg(R)	20.842	22.5	22.38
A1g(R)	11.495	12.5	12.34
A1g(R)	18.272	19.4	19.07
A2g	8.30		9.04
A2g	15.27		16.08
A2g	20.84	-	22.41
A1u	16.941	-	17.82
A1u	19.754	-	20.62

ture. The θ-alumina consists of a mixture of tetrahedral (50%) and octahedral (50%) aluminum cations. The presence of tetrahedral cations is responsible for larger density of phonon branches above 18 THz. The average Al-O bond equals $d_O=1.95$ Å for an octahedrally coordinated cation and only $d_T=1.77$ Å for tetrahedral Al. The shorter bonds contribute to the higher frequency spectrum. In particular modes related to the ''breathing'' of AlO_4 are very interesting as they shall be common for variety of compounds containing AlO_4.

The extensive Raman measurements[17] of the magnesium spinels ($MgAl_2O_4$) reveal the following features that are directly related to the AlO_4 breathing modes. The spinel cations can occupy two sublattices: Mg tetrahedral sites and Al octahedral interstices. A substantial difference between natural and synthetic $MgAl_2O_4$ was found[17] in the high energy part of the Raman spectrum. The peak around 21.8 THz is present in the synthetic spinel, while in natural samples it appears only when they are heated up to 1300 K and quenched rapidly. It was suggested[17] that the disorder in the cation sublattice is responsible for this effect. Some of the Al cations migrate to the tetrahedral sites and form AlO_4, giving an additional peak at 21.8 THz.

TABLE III. The frequencies (in THz) of the optical modes of the θ-Al_2O_3 at $\mathbf{q}=\Gamma$. The experimental value is taken from data for magnesium spinel. Only TO frequencies are shown for infrared modes.

Mode	Present	Expt. (Ref.17)
Au(I)	7.974; 9.894; 14.349; 21.136	-
Bu(I)	9.634; 10.650; 12.649; 14.534	-
Bu(I)	16.339; 18.061; 21.223; 22.483	-
Ag(R)	5.966; 7.841; 8.659; 13.025; 13.092	-
Ag(R)	15.842; 17.879; 20.403; 23.465	
Ag(R)	20.758	21.79
Bg(R)	5.824; 6.822; 11.480; 14.872; 20.889	-

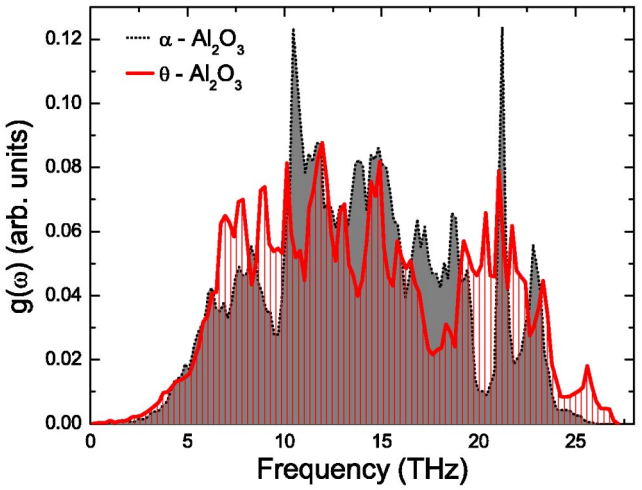

FIG. 3. (Color online) Total density of phonon states for α (gray shaded region) and θ (thick, solid red lines) phases of Al_2O_3. The DOS $g(\omega)$ is normalized $\int g(\omega)d\omega=1$.

The structure of θ-alumina gives a direct insight into AlO_4 dynamics, since this AlO_4 unit exists directly in this phase, such that no further approximations are required in contrast to the $MgAl_2O_4$ system.[18] In that sense, we may relate two Raman modes of A_g symmetry at 20.758 and 23.465 THz, which are AlO_4-tetrahedron breathing and stretching of the Al^T-O bond, respectively, to the same modes in the spinel structure. The close agreement between these frequencies, and their common origin from the tetrahedrally coordinated Al, point to the high stability of such coordination, despite the very different chemical environment.

B. Density of states

The difference in the vibrational spectrum of both phases is better visible on the density of states (DOS) plots, presented in Fig. 3. The spectrum of corundum develops two prominent Van Hove peaks at 10.4 and 21.2 THz. 67% of $g(\omega)$ ranges from 9.5 to 20 THz, while 20% has a lower frequency. The $g(\omega)$ of the θ phase, on the other hand, possesses two distinct regions dividing the spectrum into separate parts below and above 18 THz. The lower part of the spectrum contains 70% of $g(\omega)$.

Another interesting point is the rich structure of the high frequency region of the DOS in the θ phase, which can be ascribed to AlO_4 vibration. Overall the DOS of θ-Al_2O_3 extends 2 THz above the DOS of corundum. The differences in $g(\omega)$ suggest different vibrational contributions to the free energy in both phases.

C. Free energy

The small difference of the ground state energy between the considered phases of alumina raise the question of whether there is another mechanism for the stabilization of corundum from transition phases. One possibility points to the larger entropic contribution to the free energy in the case of corundum. The density of states calculated above provides a basis for further analysis in a quasiharmonic approximation.

To compare the stability of the two phases of alumina at the given thermodynamic conditions (p,V,T) one must go beyond the ground state and calculate of the free energy $G(p,T)=F(V,T)+pV$. The standard procedure is to determine Gibbs free energy $G(p,T)$; however, for our purpose the comparison of the Helmholtz free energy $F(V,T)$ is sufficient, since the corundum only exists in the crystalline phase and we are interested in the region of ambient pressures $p=p_0$.

High pressure $(p \gg p_0)$ transformations of corundum, which indeed require a direct treatment of the Gibbs free energy, were previously performed by Thomson *et al.*[19] They predicted orthorhombic Rh_2O_3 (II) structure to be the most stable above $p=75$ GPa, which was confirmed later experimentally.[20] This exemplifies the great predictive power of DFT calculations applied to alumina, but the area of high pressures is beyond the scope of the present paper. We limit our discussion here to temperature induced transformations. To account for the validity comparison of $\Delta F(V,T)$ only, the Grüneisen parameter γ_G was estimated for corundum by calculating the vibrational spectrum at a volume reduced by 3%. The value of γ_G ranges from $\gamma_G=0.4$ for the E_u mode to $\gamma_G=1.8$ for the A_{2u} mode. The average Grüneisen parameter $\langle \gamma_G \rangle = 1.14$ gives the thermal expansion coefficient $\alpha_T = 6$ ppm, which is rather small, so a comparison of the Helmholtz free energy is sufficient for our purposes. Within this limitation the Helmholtz free energy $F(V,T)$ is calculated as

$$F(V,T)=E_0(V)+F_{vib}(V,T), \tag{3.1}$$

where $E_0(V)$ is the total energy evaluated from the first principle calculations (cf. Table I). The vibrational contribution to the free energy equals

$$F_{vib}(V,T)=U(V,T)-TS(V,T), \tag{3.2}$$

where $U(V,T)$ describes the internal energy of the lattice including zero point vibrations, while the last term is for the entropic contribution. When the phonon modes are populated according to the Bose-Einstein statistics the internal energy equals

$$U(V,T)=\int_0^\infty g(\omega)\hbar\omega \coth\left(\frac{\hbar\omega}{2k_BT}\right)d\omega. \tag{3.3}$$

k_B is the Boltzmann constant. Other thermodynamic functions are calculated taking $S=0$ at $T=0$ from the third law of thermodynamics. The free energy of the system reads

$$F_{vib}(V,T)=\int_0^\infty g(\omega)\ln\sinh\left(\frac{\hbar\omega}{2k_BT}\right)d\omega. \tag{3.4}$$

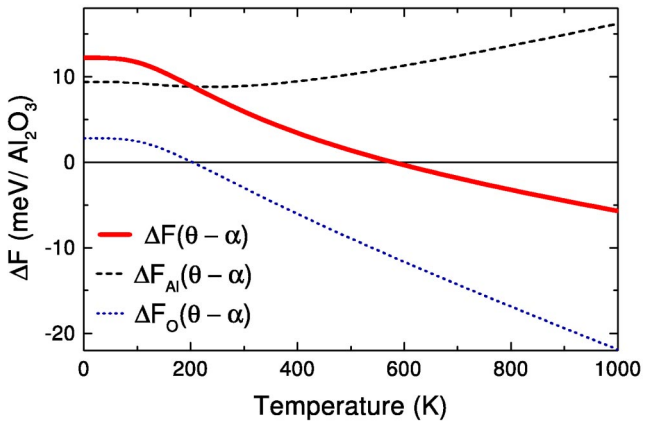

FIG. 4. (Color online) The difference of the vibrational part of the free energy $\Delta F_{vib}(\theta-\alpha)$ (thick, solid red line). The partial contributions coming from anionic (dotted blue) and cationic (dashed black) subsystems are also shown.

The difference of the vibrational free energy $\Delta F_{vib}(\theta-\alpha)$ is presented in Fig. 4. The zero point energy contribution to the free energy of the θ phase is larger at $T=0$ K, confirming the stability of the corundum at low temperature. With increasing temperature entropy decreases the stability of this phase, driving the θ-Al_2O_3 to be more stable above $T=590$ K. This stabilization is, however, not sufficient to convert the system toward the θ phase unless the temperature rises well above the melting point as the static energy difference ΔE must be taken into account. Nevertheless transition aluminas do not exist in the crystalline state and there must be additional stabilization mechanisms related to their porosity. One must also be aware of several limitations of above approach. First of all local anharmonic effects related, at first, to the significant mode coupling, could play a role of further decreasing the $F_{vib}(\theta)$. Second, transition aluminas possess large surface areas. Corundum usually does not exist in such a porous state, but even the porous α-alumina holds significantly smaller surface areas (up to 100 m^2/g). McHale *et al.*,[21] when comparing the stability of porous γ and α phases, suggested that the lower surface energy of transition alumina is responsible for its stabilization. This interesting point is still awaiting direct confirmation.

Besides all the limitations, the picture of entropy driven destabilization of corundum, presented above, is clear and shows an important mechanism contributing to the stability of the transition aluminas over a wide range of temperatures. This also indicates that the dense θ-alumina is not a ground state of Al_2O_3.

IV. DISCUSSION

The calculations give the opportunity for a strict division of the entire vibrational spectrum into partial contributions, so that further analysis is possible, as there is no energy exchange between modes in harmonic systems. The reader must be aware that this is not the case in real systems, where, at equilibrium, energy is shared equally between all modes. The following analysis is justified, however, as it shows

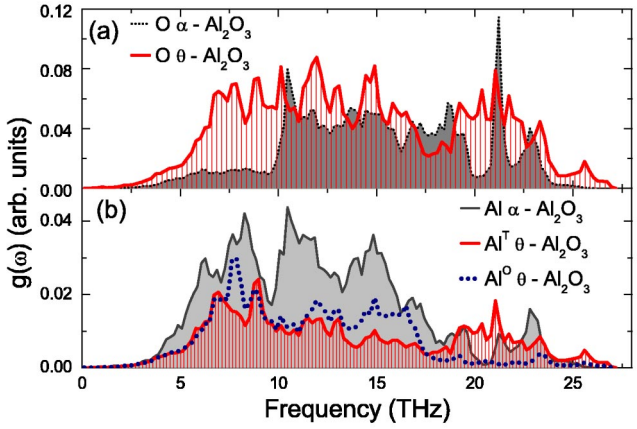

FIG. 5. (Color online) Partial densities of states. (a) Oxygen sublattice of corundum (gray shaded) and θ-alumina (thick, solid red lines). (b) Aluminum sublattice. The gray shaded region is for Al^O of corundum, and solid red lines are for Al^O, dotted blue for tetrahedral cations of θ-Al_2O_3.

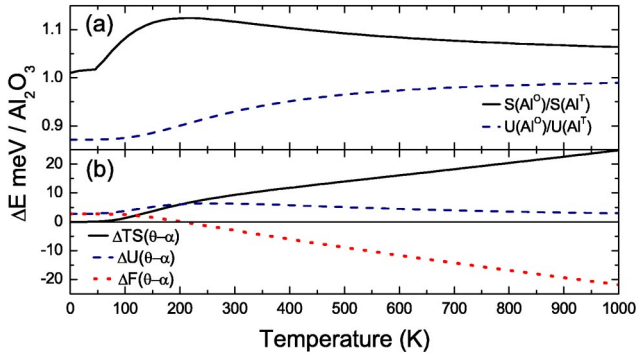

FIG. 6. (Color online) Temperature dependence of the vibrational free energy ΔF_{vib}, entropy ΔS, and internal energy ΔU. (a) Ratio between U and S of tetrahedral and octahedral cation subsystems of θ phase. (b) Difference between fcc and hcp oxygen sublattices. ΔF_{vib} is dotted red, ΔS is solid black, and ΔU is dashed blue.

which modes are primarily excited prior to achieving equilibrium and possibly contribute to structural modifications.

It is very instructive to examine closer the differences of the free energy distribution between both phases of alumina and even going further to compare partial contributions coming from different sublattices. The partial densities of states for aluminum and oxygen are presented in Fig. 5. The vibrations of oxygen arranged in the hcp sublattice in corundum are limited mainly to the region between 10 and 20 THz, with small contribution from the acoustic branches and high energy excitations. The partial DOS that results from the fcc arranged oxygen in the θ phase looks rather different. It spans the same frequency range as the total DOS, and has a similar shape.

The cationic sublattice of corundum covers majority of excitation of modes below 10 THz; see Fig. 5(b). Weak and fairly localized modes are present at high frequencies. They belong to the Al-O stretching, giving two peaks around 23 THz.

The spectrum of tetrahedral and octahedral Al in the θ phase reveals their difference. While the $g(\omega)$ for Al^O follows that of corundum closely, almost all of the high frequency phonons belong to the tetrahedral subsystem. This shows the stability of the AlO_4 configuration. The high frequency Al-O stretching modes are also present in the θ phase but at higher frequencies and here they are surrounded by other excitations.

The distribution of internal energy and entropy between presented subsystems depends on the differences of the $g(\omega)$. Figure 6(a) shows the distribution of the internal energy U and entropy S between Al^O and Al^T. At the low temperature limit, a larger amount of the U belongs to tetrahedral subsystem. At high temperatures, U equilibrates between subsystems. The vibrational entropy S is always larger for the Al^O subsystem. This stabilizes the octahedral subsystem and the vibrational free energy is always lower for it. This shows that the octahedral coordination of Al is always dynamically more stable, even in the θ phase. Now comparing the cation sublattice of the two phases (Fig. 4) one can see that the pure octahedral Al coordination possesses a lower F_{vib} at every temperature. But anionic/cationic subsystems do not exist separately. Only 40% of the internal energy is carried by cations.

Comparing the internal energy between hcp and fcc sublattices of oxygen [see Fig. 6(b)], we notice they are almost equal, slightly favoring hcp arrangements in the low temperature limit. With increasing temperature the difference slightly grows, until the modes above 10 THz are excited in the hcp structure. This leads to the equilibration of U toward higher T, as shown in Fig. 6(b). The entropy of the fcc oxygen arrangement is larger at all temperatures and the difference $S(\text{fcc}-\text{hcp})$ grows continuously. Around $T\sim 200$ K, entropy wins against internal energy and the fcc structure of oxygen becomes more stable; see Fig. 6(b). The differences in the free energy are quite small, so they cannot be responsible for transformations between structures, but the tendencies are well described, as they become more visible as the temperature rises.

The picture of the stability between phases shows that the free energy of the octahedral arrangement of aluminum contributes to the stabilization of this coordination at all temperatures. This, together with a lower free energy of the hcp anionic sublattice, stabilizes α-Al_2O_3 in the low temperature limit. At higher T, the large vibrational entropy of fcc oxygen in θ-Al_2O_3 counteracts the stabilization coming from cations and the stability shifts toward the transition phase. An oxygen arrangement different than hcp is always accompanied by the presence of tetrahedral Al cations.

This is a very interesting point that explains the common occurrence of the tetrahedrally coordinated aluminum in the variety of aluminas. There is a simple correlation between the presence of Al^T and the structure of the oxygen sublattice. In the structure of corundum, oxygen possesses *ABABAB* (hcp) stacking and no tetrahedral cations are present. In the κ phase[22] the oxygen stacking is *ABAC*, and thus different from hcp and fcc. In this structure, 25% of cations are tetrahedrally coordinated. In the θ-Al_2O_3, stacking of oxygen is *ABCABC*, and as many as 50% of cations

occupy tetrahedral positions. In fact the presence of tetrahedral Al should not be stable from the dynamical point of view. However, tetrahedral Al is responsible for the stabilization of an oxygen arrangement other than hcp. The low free energy of this arrangement at high temperatures forces aluminum to occupy tetrahedral sites.

An intriguing result was presented in Ref. 5, where the tendency of aluminum to occupy the tetrahedral position in the spinel structures of alumina was shown by means of DFT calculations. This result is along the line of our finding of the stabilizing role of oxygen in aluminas with fcc oxygen lattice. The stabilization of the spinel is more complicated, as the presence of vacancies in the structure plays an important role.

Thin alumina films grown on an NiAl substrate contain significant amounts of Al^T.[23,24] The CVD-grown, high resistive coatings usually consist of the alumina in the κ phase,[22] which contains 25% of Al^T. In all these examples, the presence of Al^T appears to stabilize an oxygen structure different from hcp, and the oxygen arrangement is a factor that determines the presence of tetrahedral aluminum cations. In the thin layers the surface contribution to the overall stability cannot be neglected, and work to resolve its role is in progress. Also the coordination of aluminum in the melt of Al_2O_3 shows an abnormal abundance of tetrahedrally coordinated cations. This liquid phase is different from the crystalline, but Al^T is not a surprise.

V. CONCLUSION

By calculating the phonon dispersion relations and the density of states for two important phases of alumina, α and θ, we have shown that the vibrational contribution to the free energy leads to a destabilization of corundum at high temperatures. Destabilization only by the vibrational effect is not sufficient to drive the structural transition between those phases. The question of the stability of the transition aluminas is still open, and is the subject of our studies.

We have shown that at low temperatures the structure of corundum, besides an electronic contribution, is stabilized by the hcp arrangement of the oxygen sublattice. At high temperatures the entropy of the fcc oxygen sublattice entails a stability shift toward this configuration. This induces the appearance of Al^T, which stabilizes the fcc arrangement of oxygen. It explains the very common presence of tetrahedral cations in a variety of aluminas, ranging from thin films to the transition phases.

The presence of tetrahedral cations associated to the fcc oxygen arrangement partially contributes to the stabilization of the metastable aluminas. However, in the quasiharmonic approximation, the stabilization of the θ phase cannot come only from the vibrational entropy. Another mechanism, possibly related to the surface, must be responsible for the stabilization.

ACKNOWLEDGMENTS

The authors would like to thank J. K. Nørskov for stimulating discussions and S. C. Parker for reading the manuscript. CAMP is sponsored by the Danish National Research Foundation.

[1] K. Wefers and C. Misra, *Oxides and Hydroxides of Aluminium*, Alcoa Technical Paper No 19 (revised), Alcoa Laboratories (1987).
[2] V. E. Heinrich and P. A. Cox, *The Surface Science of Metal Oxides* (Cambridge University Press, Cambridge, 1994).
[3] I. Levin and D. Brandon, J. Am. Ceram. Soc. **81**, 2012 (1998).
[4] R.-S. Zhou and R.L. Snyder, Acta Crystallogr., Sect. B: Struct. Sci. **47**, 617 (1991).
[5] C. Wolverton and K.C. Hass, Phys. Rev. B **63**, 024102 (2001).
[6] G. Gutiérrez, A. Taga, and B. Johansson, Phys. Rev. B **65**, 012101 (2001).
[7] G. Kresse and J. Furthmüller, computer code VASP (Vienna, Austria, 1999), Comput. Mater. Sci. **6**, 15 (1996).
[8] J.P. Perdew, J.A. Chevary, S.H. Vosko, K.A. Jackson, M.R. Pederson, D.J. Singh, and C. Fiolhais, Phys. Rev. B **46**, 6671 (1992).
[9] K. Parlinski, computer code PHONON (Kraków, Poland, 2002).
[10] K. Parlinski, Z.Q. Li, and Y. Kawazoe, Phys. Rev. Lett. **78**, 4063 (1997).
[11] R. Heid, D. Strauch, and K.-P. Bohen, Phys. Rev. B **61**, 8625 (2000).
[12] W.E. Lee and K.P.D. Lagerlof, J. Electron Microsc. Tech. **2**, 247 (1985).
[13] A.S. Baker, Jr., Phys. Rev. **132**, 1474 (1963).
[14] F. Grevais and B. Piriou, J. Phys. C **7**, 2374 (1973).
[15] H. Schober, D. Strauch, and B. Dorner, Z. Phys. B: Condens. Matter **92**, 273 (1993).
[16] M. Schubert, T.E. Tiwald, and C.M. Herzinger, Phys. Rev. B **61**, 8187 (2000).
[17] H. Cynn, S.K. Sharma, T.F. Cooney, and M. Nicol, Phys. Rev. B **45**, 500 (1992).
[18] G.A. de Wijs, C.M. Fang, G. Kresse, and G. de With, Phys. Rev. B **65**, 094305 (2002).
[19] K.T. Thomson, R.M. Wentzcovitch, and M.S.T. Bukovinski, Science (Washington, DC, U.S.) **274**, 1880 (1996).
[20] N. Funamori and R. Jeanloz, Science (Washington, DC, U.S.) **278**, 1109 (1997).
[21] J.M. McHale, A. Auroux, A.J. Perrotta, and A. Navrotsky, Science (Washington, DC, U.S.) **277**, 788 (1997).
[22] Y. Yourdshahyan, C. Ruberto, M. Halvarsson, L. Bengtsson, V. Langer, and B. Lundqvist, J. Am. Ceram. Soc. **82**, 1365 (1999).
[23] A. Bogicevic and D.W. Jennison, Surf. Sci. **464**, 108 (2000).
[24] A. Stierle, V. Formoso, F. Comin, and R. Franchy, Surf. Sci. **467**, 85 (2000).